Two Distinct Regimes in the Kinematic and Thermodynamic Structure of the Hurricane Eye and Eyewall

JAMES P. KOSSIN AND MATTHEW D. EASTIN

Department of Atmospheric Science, Colorado State University, Fort Collins, Colorado

(Manuscript received 10 August 1999, in final form 22 August 2000)

ABSTRACT

Using aircraft flight-level data, the present work demonstrates that the kinematic and thermodynamic distributions within the eye and eyewall of strong hurricanes are observed to evolve between two distinct regimes. In the first regime, angular velocity is greatest within the eyewall and relatively depressed within the eye. In the second regime, radial profiles of angular velocity are nearly monotonic, with maxima found at the eye center. Considering sequential profiles within individual hurricanes, the authors find that the evolution of the kinematic distribution is often marked by a transition from the first regime to the second. The transition can occur in less than 1 h.

Also noted during the transition are dramatic changes in the thermodynamic structure of the hurricane. Prior to the transition (regime 1), the eye is typically very warm and dry, and the equivalent potential temperature is often elevated within the eyewall and relatively depressed within the eye. After the transition (regime 2), eye temperatures may be lower, higher, or unchanged; dewpoints are higher; and equivalent potential temperature profiles are often nearly monotonic with maxima at the hurricane center.

A mechanism is suggested, based on horizontal vorticity mixing, whereby the observed transitions within the hurricane eye and eyewall might be well explained within an idealized 2D barotropic framework.

1. Introduction

Previous studies based on dropsonde data in hurricanes have shown that distinct transitions often occur in the vertical thermodynamic structure of the eye. Jordan (1961), Franklin et al. (1988), and Willoughby (1998) demonstrated that intensifying hurricanes typically have warm, dry eyes above a marked inversion level that tends to descend during intensification, while during weakening, the inversion level typically ascends and the eye soundings become more moist.

The motivation for the present study is threefold. 1) By employing flight-level data, we can observe changes in the radial structure of the thermodynamic fields across the hurricane eye and eyewall. 2) The availability of flight-level wind data allows observation of changes in the *radial* profiles of kinematic and dynamic variables. 3) We present evidence that horizontal mixing between the eye and eyewall may explain the observed evolution of the thermodynamic and kinematic fields.

In section 2a, we consider sequential flight legs in individual hurricanes and find that radial profiles of kinematic variables evolve between two distinct regimes. In the first regime (regime 1), which is typically indicative of intensifying hurricanes, angular velocity is significantly enhanced within the eyewall and relatively depressed in the eye and outside the eyewall. The transition to the second regime (regime 2), which typically occurs just after maximum intensity, is marked by dramatic changes in the angular velocity distributions and can occur over a period of a few hours or less. During the transition, angular velocity profiles become nearly monotonic across the eye and eyewall as maxima within the eyewall weaken considerably, while angular velocity within the eye increases. The tangential winds (and angular momentum) increase within the eye as the local angular velocity increases.

Concurrent with changes in the kinematic fields, the transition to regime 2 is often marked by dramatic changes in the thermodynamic structure within the eye and eyewall. This is discussed in section 2b. We find that in regime 1, profiles of temperature and dewpoint typically indicate very warm and dry eyes, and equivalent potential temperature (θ_e) profiles often exhibit maxima within the eyewall. During the transition to regime 2, dewpoints increase appreciably and the maxima of θ_e often apparent within the eyewall in the first regime tend to vanish as the profiles become monotonic with maxima at the eye center.

In section 2c, a mechanism is suggested whereby the

Corresponding author address: James P. Kossin, Department of Atmospheric Science, Colorado State University, Fort Collins, CO 80523.
E-mail: kossin@euler.atmos.colostate.edu

transition from regime 1 to regime 2 might be explained independently of vertical displacements of the inversion level in the eye. We consider asymmetric horizontal mixing, as described by Schubert et al. (1999), and find that much of the observed physics can be understood in the highly idealized 2D barotropic framework.

2. Results

The work presented here utilizes flight-level data from the National Oceanic and Atmospheric Administration (NOAA) Hurricane Research Division archive of aircraft observations collected over 20 yr (1977–96) from 44 Atlantic and eastern Pacific hurricanes. The data were collected by two NOAA WP-3D research aircraft and the Air Force 53rd Weather Reconaissance fleet of WC-130 aircraft. A formal description of the data processing and WP-3D instrumentation is found in Jorgensen (1984). Instrumentation on board the WC-130 aircraft is nearly identical to that of the WP-3D aircraft but the data recording frequency is 0.1 Hz on the WC-130 versus 1.0 Hz on the WP-3D. The accuracies of the horizontal winds (tangential and radial) are ± 1.0 m s^{-1} and ± 2.0 m s^{-1} for the WP-3D and WC-130 aircraft, respectively (OFCM 1993). The database consists of storm-relative observations of the three-dimensional wind field[1] in cylindrical coordinates translating with the hurricane center, temperature, dewpoint, geopotential height, and the aircraft location given in latitude and longitude, partitioned into radial legs. A radial leg is defined as either an inbound flight path toward the storm center, or an outbound path away from the storm center. Data within each radial leg are distributed into 0.5-km average bins. The radial legs used in this study were flown along the 850-, 700-, 600-, and 500-mb constant pressure surfaces.

The results presented in sections 2a,b are based on Hurricanes Diana (1984) and Olivia (1994). Our findings in these two specific cases are, however, markedly robust and representative of a larger group of hurricanes.

a. Transitions in kinematic distributions

During the 36-h period, 1200 UTC 10 September to 0000 UTC 12 September 1984, Atlantic Hurricane Diana intensified from a minimal category 1 to a category 4 hurricane. Aircraft observations along the 850-mb pressure surface during the period of intensification (Fig. 1a) were indicative of regime 1, exhibiting enhanced angular velocity in the eyewall and depressed angular velocity in the eye. After 0000 UTC 12 September, while approaching the east coast of the Carolinas, Diana weakened and became a category 2 hurricane in the next 6 h. Within 1 h after the cessation of intensification, the observed angular velocity profiles changed dramatically, becoming nearly monotonic (Fig. 1b) as described by regime 2. The angular velocity within the eyewall generally decreased while the angular velocity in the eye generally increased.

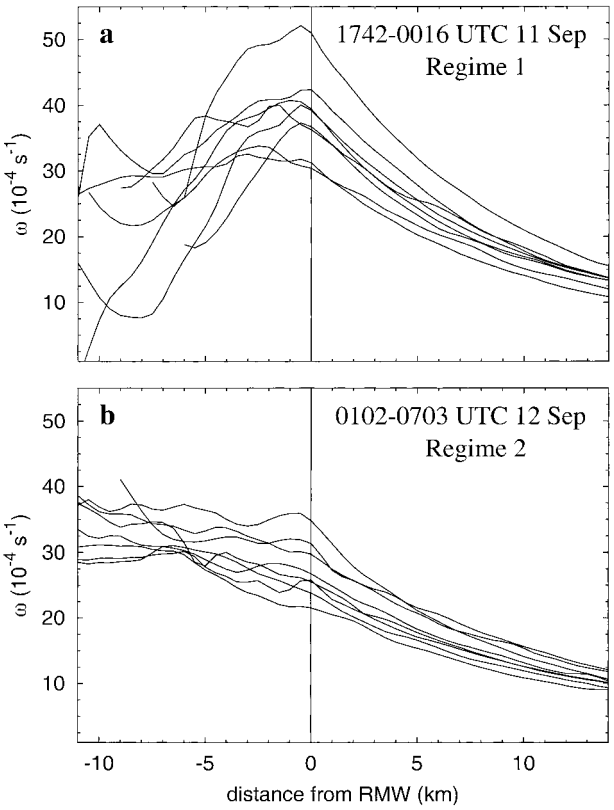

FIG. 1. Observed flight-level angular velocity at 850 mb in Hurricane Diana (1984). Each angular velocity profile is positioned with respect to distance from the radius of maximum tangential wind (RMW) for that particular radial flight leg. Negative distance represents distance inward (into the eye) from the RMW. (a) Eight radial legs flown prior to maximum intensity during 1742–0016 UTC 11–12 Sep. The profiles are indicative of regime 1. (b) Eight radial legs flown subsequent to maximum intensity during 0102–0703 UTC 12 Sep. The profiles are indicative of regime 2 and represent nearly solid body rotation across the eye and eyewall. Note the general decrease in angular velocity at the RMW (in the eyewall) concurrent with the general increase inside the RMW (in the eye).

During the transition to regime 2, the radius of maximum tangential wind (RMW) remained relatively fixed and although the maximum wind decreased, the tangential flow in the eye increased. Figure 2 displays the evolution of flight-level tangential wind observed at 5 km from Diana's center (in the eye) and the maximum wind observed (in the eyewall). While inaccuracies in the acquisition of winds near the eye center can arise due to less than perfect center fixes, the trend appears to be that of increasing tangential flow in the eye concurrent with decreasing tangential flow in the eyewall. The maximum wind decreased after 2100 UTC 11 September, as expected during weakening. The flow at $r =$

[1] Observations taken by the WC-130 aircraft include only horizontal winds.

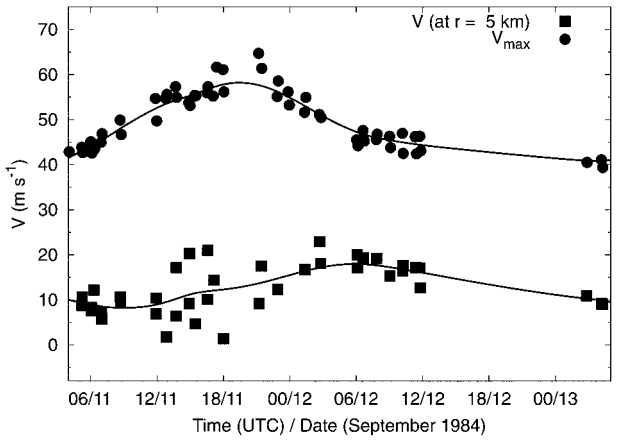

FIG. 2. Flight-level tangential wind at 850 mb in Hurricane Diana (1984) observed from 0400 UTC 11 Sep to 0500 UTC 13 Sep. Squares represent the wind 5 km from the hurricane center (in the eye) and circles represent the maximum wind (in the eyewall).

5 km (in the eye) after 2100 UTC was observed to increase, and reached a maximum roughly 10 h after the maximum eyewall winds were recorded. Observations beyond 0700 UTC 12 September indicate steady spindown of both the maximum wind and the wind at $r = 5$ km.

Pacific Hurricane Olivia (1994) intensified from a tropical storm at 0000 UTC 23 September to its maximum strength as a category 4 hurricane around 1200–1800 UTC 25 September. After 1200–1800 UTC 25 September, Olivia weakened steadily while moving northward over cooler water. Analogously to Hurricane Diana at 850 mb, Olivia's flight-level angular velocity profiles at 600 mb were indicative of regime 1 during intensification (Fig. 3a). At some time during the period 2210–2249 UTC, while Olivia was weakening, the transition from regime 1 to regime 2 became evident in the flight-level data as the flow within the eyewall and eye relaxed toward solid body rotation (Fig. 3b). Concurrent with the transition was a marked spinup of the tangential flow in the eye.

b. Transitions in thermodynamic distributions

The relationship between intensity change and changes in the vertical thermodynamic structure of the hurricane eye has been well documented using aircraft dropsonde data. Jordan (1961) found that intense typhoons typically exhibited unusually warm and dry eyes during periods of intensification, while subsequent to maximum intensity, eye soundings often transitioned toward moist adiabatic. Franklin et al. (1988) noted remarkable changes in temperature and moisture soundings in Hurricane Gloria (1985) during rapid intensification. Both studies found the thermodynamic changes to be associated with vertical displacement of the inversion level in the eye.

The contribution to the changes in vertical structure

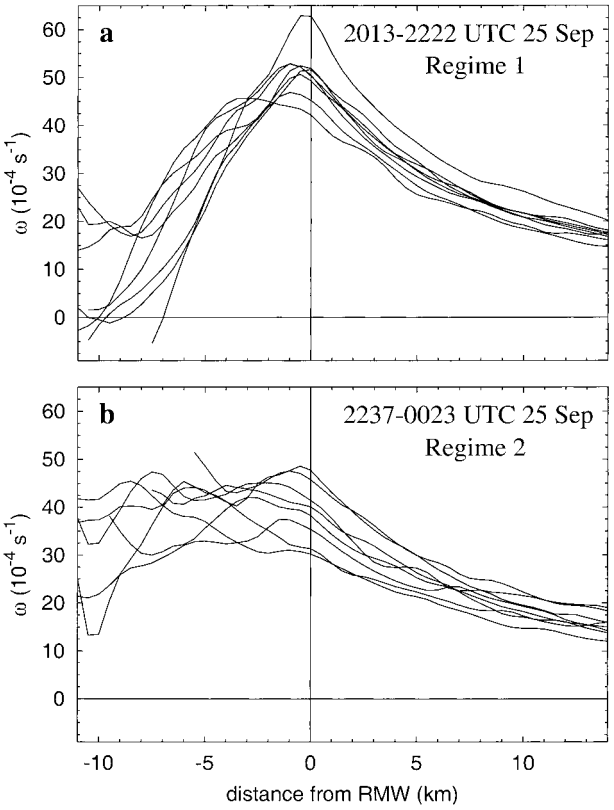

FIG. 3. Similar to Fig. 1 but for Hurricane Olivia (1994) at 600 mb.

due to undilute dry adiabatic descent was considered by Franklin et al. (1988) and found to explain only part of the observed transition in Gloria. Based on their findings, they hypothesized that other factors, such as gravity waves or detrainment of moist air from the eyewall into the eye, must play a role in changes above the inversion. This hypothesis will be partially addressed in section 2c.

Here we investigate changes in the radial thermodynamic distributions across the hurricane eye and eyewall. Similarly to section 2a, we consider 850-mb flight-level data in Hurricane Diana (1984) and 600-mb flight-level data in Hurricane Olivia (1994). Equivalent potential temperature was calculated using the empirical formulas in Bolton (1980).

Concurrent with changes in the kinematic fields (section 2a), the thermodynamic fields along the 850-mb surface in Diana exhibited dramatic changes during the transition from regime 1 to regime 2. In regime 1 (Figs. 4a,b), the eye was very warm and dry with an 18°C dewpoint depression near the eye center. Profiles of θ_e consistently exhibited distinct maxima within the eyewall and local minima at the eye center. Differences between eye and eyewall θ_e were as large as 21 K. In regime 2 (Figs. 4c,d), the profiles had changed dramatically. The eye had become cooler, more moist, and saturated. Although the eye temperatures had decreased,

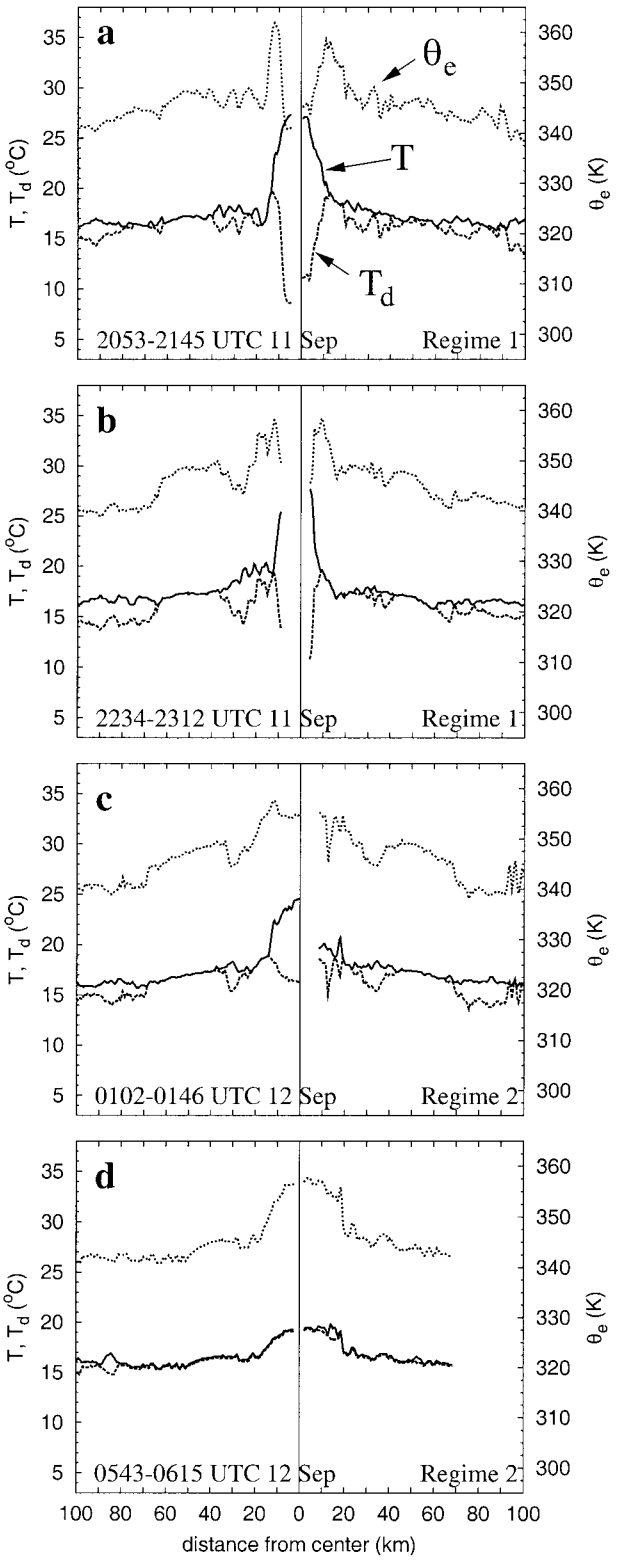

FIG. 4. Observed flight-level temperature (solid), dewpoint (long dash), and equivalent potential temperature θ_e (short dash) at 850 mb in Hurricane Diana (1984). Each panel displays two radial legs, one inbound and one outbound. The aircraft direction of flight is from left to right. The time period of each radial leg pair is at lower left.

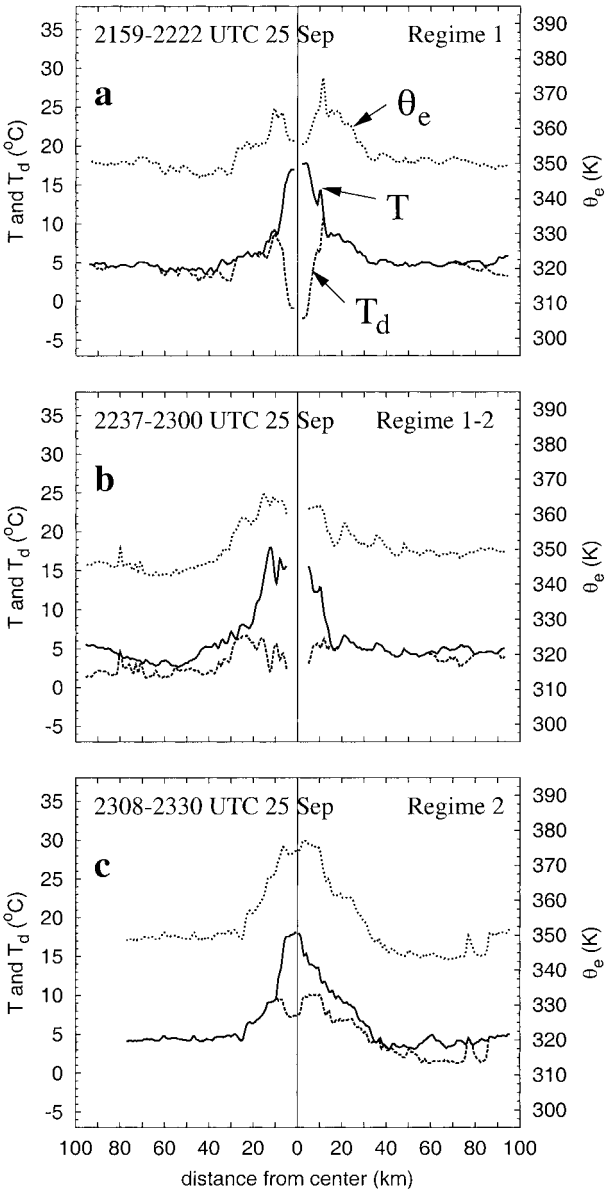

FIG. 5. Similar to Fig. 4 but for Hurricane Olivia (1994) at 600 mb. (a) Regime 1, (b) transition from regime 1 to regime 2, (c) regime 2.

the increase of dewpoint was sufficient to increase the local θ_e and the profiles had become nearly monotonic.

Profiles of thermodynamic fields in Olivia during weakening, but prior to the transition from regime 1 to 2, are shown in Fig. 5a. The eye was warm and dry with a ~20°C dewpoint depression near the eye center. Approximately 38 min later, at 2249 UTC, the aircraft

←

(a) and (b) Profiles indicative of regime 1 observed during intensification. (c) and (d) Profiles indicative of regime 2 observed during weakening, shortly after maximum intensity.

reentered Olivia's eye and appears to have captured the transitioning thermodynamic fields (Fig. 5b). During the subsequent radial leg pair, the profiles across the eye and eyewall were indicative of regime 2 (Fig. 5c). During the transition, temperatures in the eye remained roughly constant while dewpoints increased from −1°C at 2211 UTC to 3°C at 2249 UTC and to 7.5°C at 2318 UTC.

In agreement with observations of Willoughby (1998), θ_e profiles in Fig. 5a exhibited local minima in the eye and maxima in the eyewall. The difference between eyewall θ_e and θ_e near the eye center was ~10 K during the inbound radial leg and ~19 K during the outbound leg. However, as shown in Figs. 5b,c, the profiles became nearly monotonic during the transition as local dewpoints increased.

c. Transitions associated with horizontal mixing

As shown in section 2a, radial profiles of angular velocity during regime 1 exhibit maxima in the eyewall and local minima in the eye. The symmetric part of the vorticity associated with such flows often consists of an annular ring of enhanced vorticity in the eyewall with relatively weak vorticity inside (in the eye) and outside. A recent study by Schubert et al. (1999) demonstrated that such vorticity profiles can support exponential barotropic instability, and the growth of the unstable modes leads to a vigorous turbulent exchange between the eye and eyewall. This exchange brings about a rearrangement of the vorticity field where much of the enhanced eyewall vorticity is mixed into the eye while weaker eye vorticity is thrown outward. The ultimate result of this process is a relaxation of the vorticity field to a monotonic, and thus exponentially stable, state. Could this idealized model explain the observed transitions from regime 1 to regime 2?

To address this question, we first computed radial profiles of relative vorticity based on observed flight-level tangential winds. Ideally, consideration of mixing processes within the three-dimensional flow of a hurricane would be based on the evolution of potential vorticity, but the one-dimensional nature of the data constrained us to consider the symmetric vertical component of vorticity as a surrogate for potential vorticity. Understanding this limitation, the vertical component of the relative vorticity (ζ) associated with the tangential wind v in a polar coordinate system translating with the hurricane center is given by $\zeta(r, \phi) = v(r, \phi)/r + \partial v(r, \phi)/\partial r$. Noting that ϕ is roughly fixed along a radial leg, application to the flight-level data was performed using the difference formula, $\zeta(\bar{r}_i, \phi) = \bar{v}_i/\bar{r}_i + (v_{i+1} - v_i)/(r_{i+1} - r_i)$, where $\bar{r}_i = (r_i + r_{i+1})/2$ and $\bar{v}_i = (v_i + v_{i+1})/2$ and the subscripts refer to bin position. The profiles were then smoothed using a 7-point filter, which effectively removed oscillations with wavelengths less than ~4 km.

Similarly to angular velocity, vorticity profiles in Hurricane Diana were observed to remain significantly peaked in the eyewall and depressed in the eye during regime 1 (Figs. 6a,b). The transition to regime 2 was marked by a reduction of eyewall vorticity concurrent with an increase of vorticity in the eye and within a few kilometers outside the eyewall (Figs. 6c,d). The transition in the vorticity (and tangential wind) profiles may be further demonstrated by averaging all profiles observed during intensification (regime 1) and comparing the result with the average of all profiles observed after maximum intensity (regime 2). Averages were computed by aligning each radial leg according to distance from the RMW of that leg, and then calculating a simple average of a group of legs at each point. The result is shown in Fig. 7 and depicts the transition toward a monotonic vorticity profile. Also evident is the reduction in the maximum wind concurrent with a spinup of the tangential wind in the eye.

The evolution of 600-mb flight-level vorticity in Hurricane Olivia is shown in Fig. 8. Within regime 1 (Figs. 8a,b), eyewall vorticity was significantly peaked while vorticity near the eye center was close to zero. During, and after, the transition to regime 2 (Figs. 8c–e), eyewall vorticity decreased while vorticity in the eye, and within a few kilometers outside the eyewall, increased.

For comparison with the theoretical and numerical predictions of Schubert et al. (1999), we now consider vorticity redistribution in a 2D barotropic framework. Employing the pseudospectral numerical model described by Schubert et al. (1999), we integrate an initially unstable vorticity field that imitates profiles indicative of regime 1. The doubly cyclic model domain is 200 km × 200 km and the maximum Fourier mode kept after dealiasing is 170. This results in an effective resolution of 1.18 km. Diffusion was applied using an eddy mixing coefficient $\nu = 5\ \mathrm{m^2\ s^{-1}}$ and the time step was 3 s.

The initial profile of vorticity is shown by the dashed curve in Fig. 9a (the other curves in Fig. 9 will be discussed later) and describes an intense vortex with maximum tangential wind of 60 m s^{-1} at $r = 20$ km. Vorticity evolution is shown in Fig. 10 in the form of two-dimensional vorticity maps. Near the start of the experiment, the prograding vortex Rossby waves along the inner edge of the ring ($14 \le r \le 18$ km) are embedded in a local angular velocity of $\omega \approx 21 \times 10^{-4}$ s^{-1} while the retrograding waves along the outer edge of the ring ($18 \le r \le 22$ km) are embedded in stronger angular velocity of $\omega \approx 29 \times 10^{-4}$ s^{-1}. As the waves along each edge phase lock, they help each other to grow and at $t = 3$ h, the ring is visibly distorted. As the wave amplitude increases, the local differential rotation (i.e., $\partial\omega/\partial r$) further distorts the resulting asymmetries and wave breaking occurs. The breaking waves along the outer ring edge have taken the form of trailing spirals and the wavenumber 4 instability is evident along the inner ring edge.

At $t = 5.5$ h, the inner ring edge has become in-

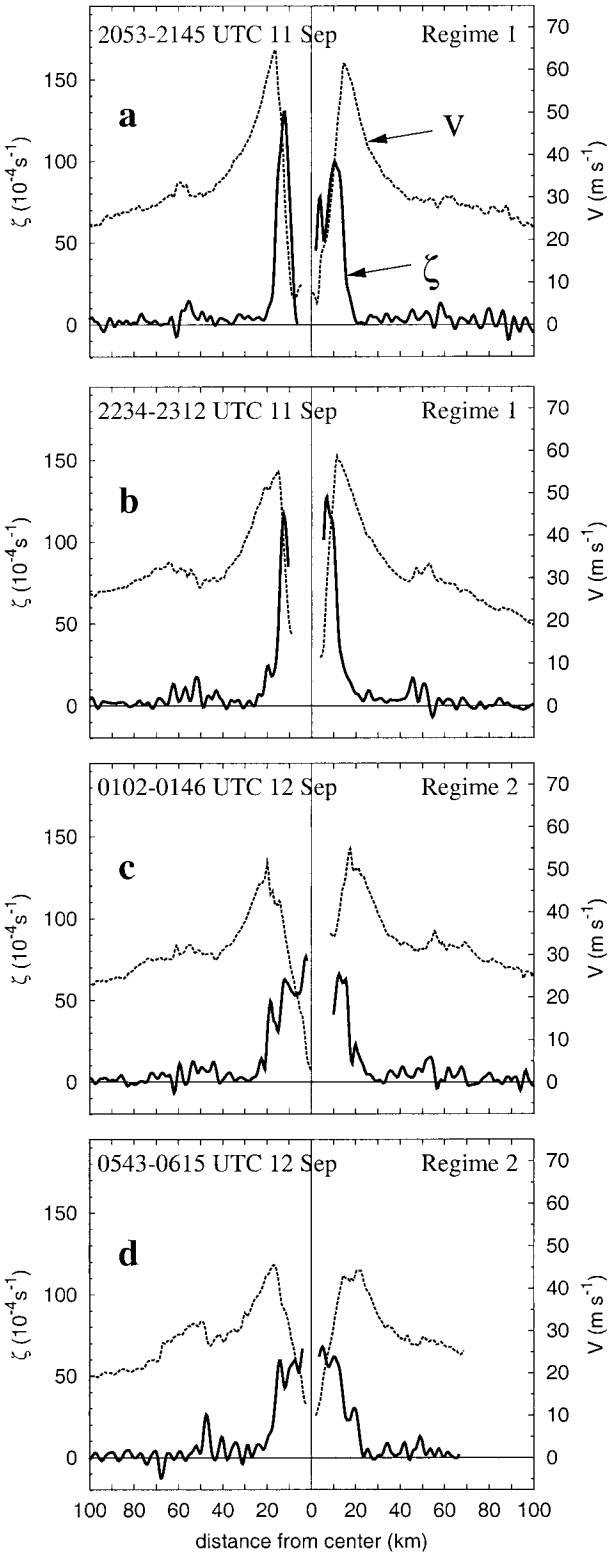

FIG. 6. Observed flight-level tangential wind (dashed) and relative vorticity (solid) at 850 mb in Hurricane Diana (1984). The time periods of the radial leg pairs in each panel are the same as in Fig. 4.

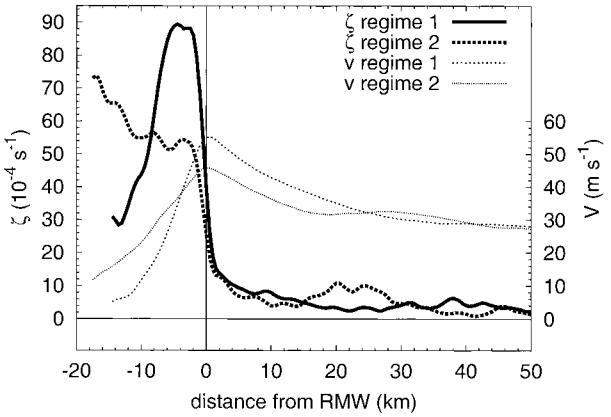

FIG. 7. Vorticity (ζ) and tangential wind (v) profiles, averaged with respect to distance from RMW, within regime 1 and regime 2 at 850 mb in Hurricane Diana (1984). Average profiles indicated as regime 1 are based on 22 radial legs flown during 1100 UTC 11 Sep to 0000 UTC 12 Sep. Average profiles indicated as regime 2 are based on 18 radial legs flown during 0000–1200 UTC 12 Sep.

creasingly distorted and coherent structures have formed that begin to migrate into the central eye region. These coherent structures might be described as ''mesovortices'' and appear to be similar in structure, location, and evolution to mesovortices observed in Hurricane Hugo 1989 (Black and Marks 1991) and Hurricane Andrew 1992 (Willoughby and Black 1996). When $t = 6$ h, a distinct mesovortex, orbiting cyclonically in the central region (eye), can be seen to the right (east) of the vortex center. As it orbits, it interacts with the coherent structures still embedded in the ring (eyewall) and as the eyewall vorticity collapses inward, intricate merger processes dominate. At $t = 12$ h, almost all of the strongest vorticity has consolidated into one structure orbiting ~5 km from the center of the domain and during the remaining 12 h of the experiment, nearly complete axisymmetrization toward a monopole occurs. The maximum vorticity within the domain remains fairly robust during the mixing process and at $t = 24$ h, the vorticity near the center is roughly 89×10^{-4} s^{-1}, which is approximately an 8% reduction of the maximum vorticity initially in the ring.

We now compare observational results in Hurricane Diana with those of the numerical experiment shown in Fig. 10. To do this, we can imagine an aircraft flying across the model domain, which we represent with a simple vorticity cross section across the inner model domain at a fixed time. The vorticity was smoothed using the same filter applied to the observed flight-level vorticity. We arbitrarily choose west to east cross sections from $x = 0$ to $x = 40$ km along the $y = 0$ line.

Cross sections of the model vorticity at $t = 0$ and $t = 12$ h are shown in Fig. 9a. At $t = 12$ h, the mixing process has resulted in a vorticity field consisting of coherent ''blobs'' embedded in a background of thin filaments. The eyewall vorticity has weakened, the eye vorticity has strengthened, and the vorticity just outside

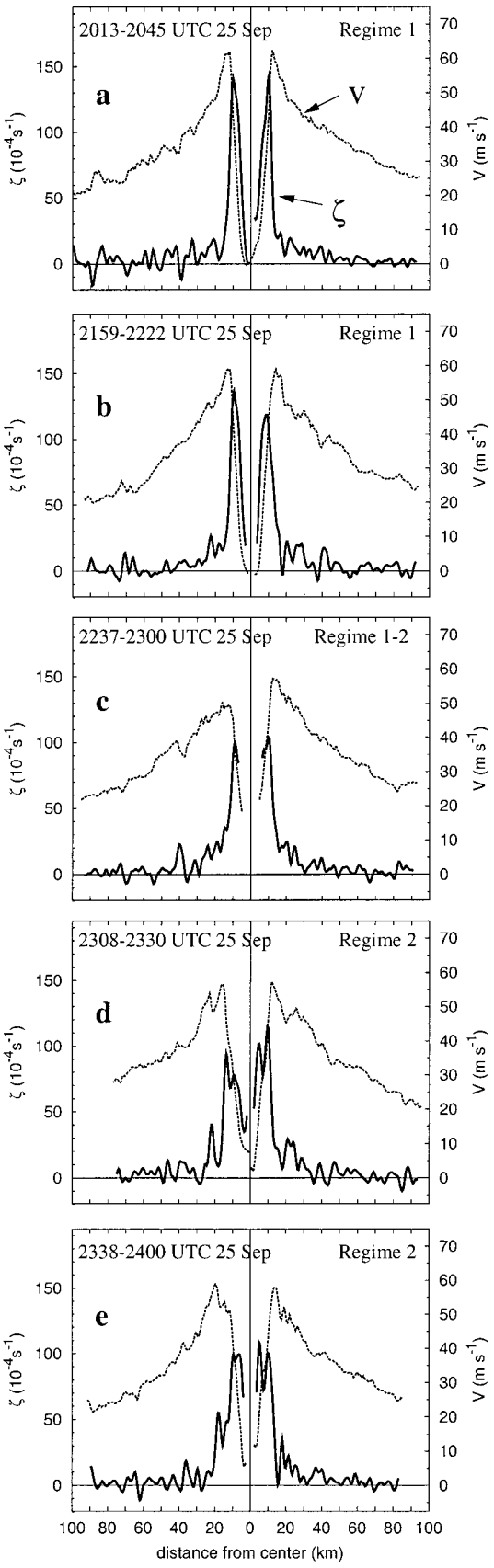

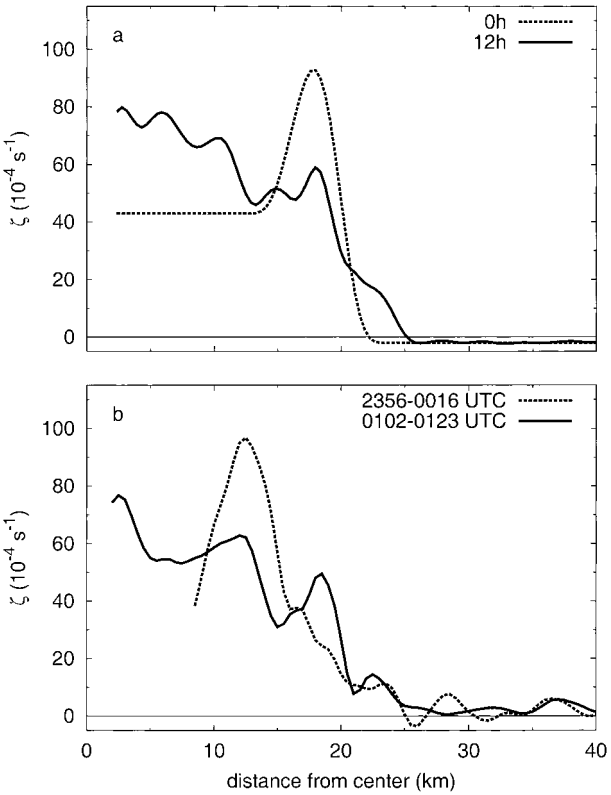

FIG. 9. (a) Cross sections of relative vorticity in the 2D barotropic model domain at $t = 0$ h (dashed) and $t = 12$ h (solid). Horizontal vorticity mixing has transported enhanced vorticity inward from the ''eyewall'' to the ''eye'' and outward to the region within a few kilometers of the original eyewall. The mixing produces vorticity filaments that create an irregular, or noisy, profile. (b) Flight-level relative vorticity observed in Hurricane Diana (1984) within regime 1 shortly before maximum intensity (dashed) and within regime 2 shortly after maximum intensity (solid). Eyewall vorticity has decreased while vorticity has increased in the eye and within a few kilometers outside the eyewall. The profiles have become more oscillatory, similarly to the numerical results.

the eyewall has increased. The profiles have, in a coarse sense, become broader and weaker while in a finer sense, the filaments, which are a ubiquitous by-product of mixing, result in a noisier profile.

As a general representation of the vorticity evolution in Diana, we consider two time periods. The first time period is 2356–0016 UTC 11–12 September and represents the flow within regime 1. The second time period is 0102–0123 UTC 12 September and represents the flow within regime 2. The vorticity profiles for each time period are shown in Fig. 9b and are notably similar, in general character, to the numerical results. The observed vorticity in Diana during the earlier time period demonstrates the peaked nature of the eyewall vorticity

←

FIG. 8. Observed flight-level tangential wind (dashed) and relative vorticity (solid) at 600 mb in Hurricane Olivia (1994).

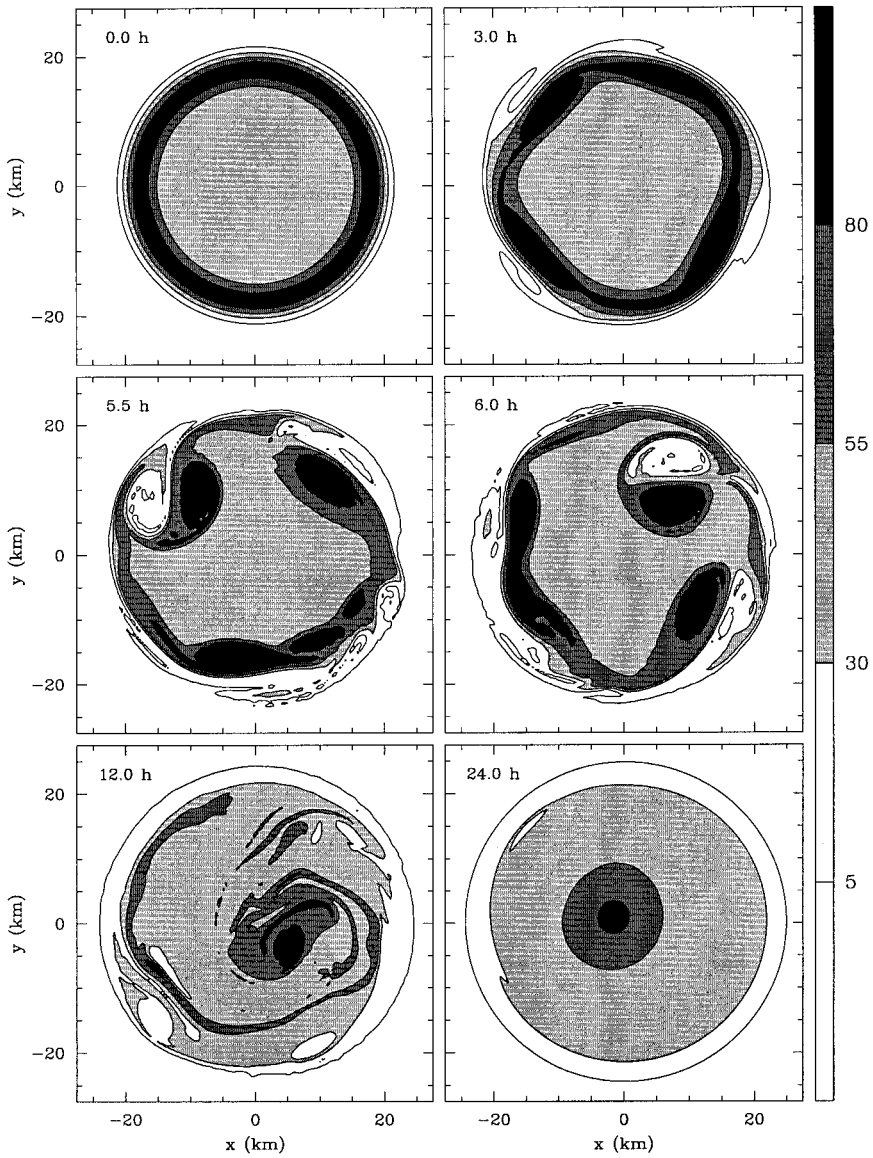

FIG. 10. Vorticity contour plots for the numerical experiment. The model domain is 200 km × 200 km but only the inner 55 km × 55 km is shown. The contours begin at 5×10^{-4} s^{-1} and are incremented by 25×10^{-4} s^{-1}. Values along the label bar are in units of 10^{-4} s^{-1}. Darker shading is associated with higher values of vorticity. Model run time in hours is shown on each plot.

in regime 1, and the profile tends to follow a fairly smooth transition from the weaker vorticity outside the eyewall, to the strongest vorticity within the eyewall, and to the weaker vorticity in the eye. In contrast, the profiles during the later time period are much less peaked. The vorticity in the eyewall region is much weaker while the vorticity near the center of the eye ($r < 5$ km) has increased substantially. The vorticity just outside the eyewall ($15 < r < 20$ km) has also experienced a substantial increase. As noted in the numerical results, the vorticity profile across the eye and eyewall has, in a coarse sense, become broader and flatter. In a finer sense, however, the profile has become more ''noisy'' and exhibits a more oscillatory structure inside $r = 20$ km. The radial scale of the oscillations observed in Diana is larger but similar to the radial scale of the filaments noted in the model domain.

While the transition apparently takes place in Diana within about an hour, the vorticity transport predicted by the numerical integration occurs more slowly. This disparity may be due to the lack of axisymmetry in an actual hurricane compared with the slightly perturbed axisymmetric initial conditions used in the model. The small pertubations applied to the modeled vorticity field

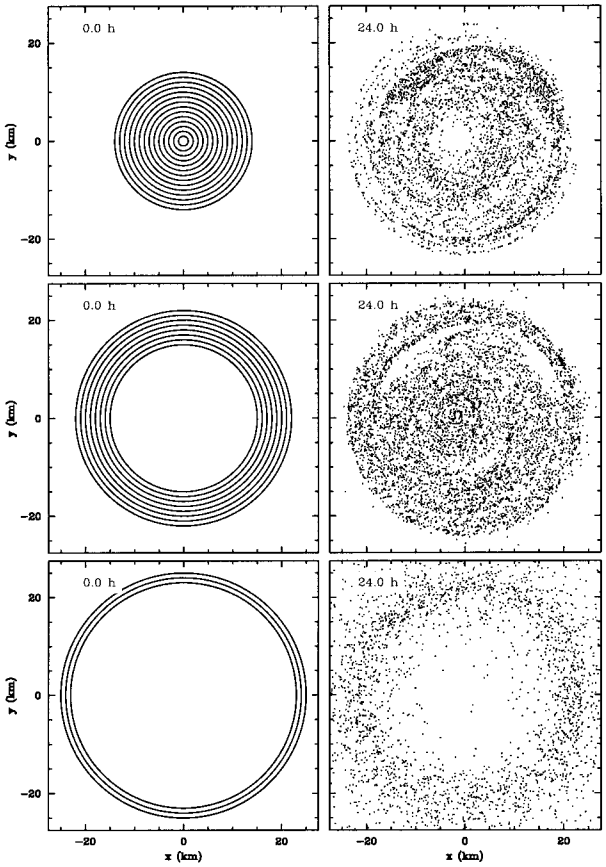

FIG. 11. Distribution of passive tracers placed in the model flow of the experiment shown in Fig. 10. Panels on the left show the initial distributions at $t = 0$ h. Panels on the right show the distributions at $t = 24$ h. The top, middle, and bottom two panels show the evolutions of tracers initially found in the eye, eyewall, and outside the eyewall, respectively.

must undergo a number of amplitude *e*-folding times before wavebreaking and mixing takes place.

The numerical evolution of a two-dimensional θ_e field may be approximated by considering the advection of passive tracers introduced into the model flow at $t = 0$ h. The tracers are initially contained along 25 concentric rings with radii $r = 1, 2, \ldots, 25$ km. The number of tracers along a concentric ring increases with increasing radius so that the number concentration of the tracers is the same along each ring. The tracer evolution is shown in Fig. 11. The top two panels show the evolution of concentric rings of tracers that were initially in the eye ($1 \leq r \leq 14$ km). At $t = 24$ h, the tracers have been completely evacuated from the central eye region inside $r \approx 4$ km and are largely found within an annulus outside $r \approx 8$ km. Two regions of relatively high tracer concentration are found in the northeast and northwest quadrants.

The middle two panels of Fig. 11 show the evolution of tracers that were initially in the eyewall ($15 \leq r \leq 22$ km). At $t = 24$ h, a large concentration of ''eyewall tracers'' are found in the eye and are particularly concentrated near $r = 0$ km. At earlier times in their evolution, the eyewall tracers entering the eye formed swirling patterns that were remarkably similar to low cloud patterns often observed in the eyes of intense hurricanes (see, e.g., Fletcher et al. 1961). Two regions of low eyewall tracer concentration are seen in the northeast and northwest quadrants. These are coincident with regions of relatively high ''eye tracer'' concentration and demonstrate that masses of air initially in the eye can remain virtually unmixed during the vorticity rearrangement.

The bottom two panels of Fig. 11 show the evolution of concentric rings of tracers that were initially outside the eyewall ($23 \leq r \leq 25$ km). At $t = 24$ h, the tracers are largely found within the annulus $15 \leq r \leq 25$ km and very few have been advected into the eye. Thus at $t = 24$ h, the central eye region is composed entirely of air that was initially in the eyewall, while the eyewall is composed of a mixture of eye and eyewall air. During the transition from regime 1 to regime 2, we might then expect that eye θ_e will increase to values initially found in the eyewall, while eyewall θ_e will decrease to a value between the initial maximum found in the eyewall and the local minimum initially found in the eye. As seen in Fig. 5, the transition does not always result in a decrease of eyewall θ_e and is thus not entirely consistent with the mixing mechanism. A possible reason for this disparity may be that the eyewall in a hurricane is being continuously diabatically forced during the transition; that is, the convection does not stop. In this case, changes in midlevel eyewall θ_e may be dependent on both horizontal mixing and changes in boundary layer θ_e.

d. Discussion

Willoughby (1998) proposed a conceptual model to explain observed changes in vertical thermodynamic structure of the eye, based on eye contraction and vertical displacement of the inversion level. In this model, the eye is considered as two distinct air masses separated by an inversion layer. The air mass below the inversion interacts freely with eyewall air (and the boundary layer). The air above the inversion may be vertically displaced a few kilometers or less as the eye expands or contracts, and exists in ''thermodynamic isolation''; that is, there is little or no exchange between interior eye air and adjacent eyewall air. Disparately, Malkus (1958) and Kuo (1959) hypothesized that subsidence in the eye occurs throughout a much deeper layer while mixing between the eye and eyewall air moistens and cools the descending air mass.

How might the results of our present work be interpreted? The transition observed to occur in Hurricane Diana (Fig. 4) was quite probably the result of a vertical displacement of the inversion level within the eye. If the inversion level within regime 1 was below 850 mb and ascended above 850 mb during the transition period,

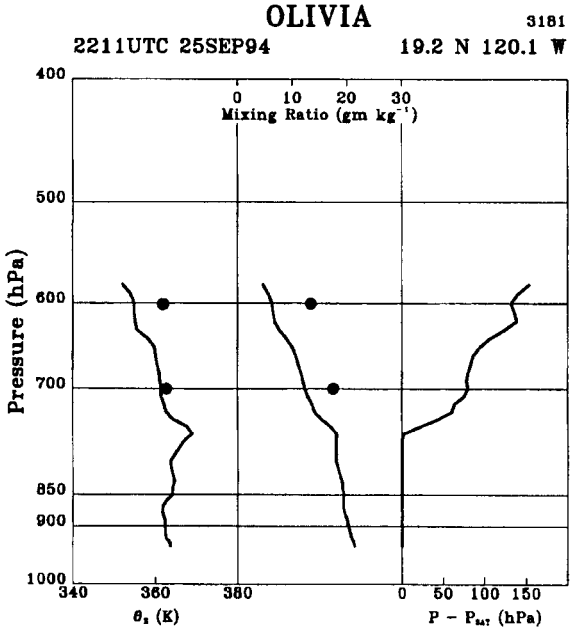

FIG. 12. Dropsonde-derived equivalent potential temperature, water vapor mixing ratio, and saturation pressure difference ($P - P_{sat}$) as functions of pressure at 2211 UTC 25 September in the eye of Hurricane Olivia (1994). The dots denote values observed at the innermost saturated point as the aircraft passed through the eyewall (reprinted from Willoughby 1998; Fig. 1d).

the observed changes could be explained in terms of ascension of a well-mixed air mass below the inversion. We found, however, that a similar transition took place at 600 mb in Hurricane Olivia and will show that the transition did not appear to be exclusively a result of an ascending inversion level.

By considering aircraft flight-level data in a select group of hurricanes, including Olivia (1994), Willoughby (1998) noted that equivalent potential temperature (θ_e) was typically observed to be higher in the eyewall than near the eye center, with θ_e differences often 10 K or more. Based in part on this observation, Willoughby argued that rapid inward mixing from the eyewall is unlikely since such mixing would be expected to eradicate the local θ_e minimum in the eye. As shown in Fig. 5, this mixing process appears to occur in Hurricane Olivia on 25 September, as θ_e near the eye center was observed to increase from 356 K at 2211 UTC to 360 K at 2249 UTC and to 377 K at 2318 UTC. A thermodynamic sounding was obtained in Olivia from a dropsonde launched in the eye at 2211 UTC (Fig. 12; see also Willoughby 1998, Fig. 1) and demonstrated that just before the transition, the maximum θ_e observed in the eye (below 600 mb) was less than 370 K, located near 740 mb. We also note from Fig. 5c that the air near the eye center at 600 mb was not saturated after the transition. The saturation pressure difference $P - P_{sat}$ (see Willoughby 1998) calculated from the 2211 UTC sounding showed the eye to be saturated from the surface to 740 mb (Fig. 12). Thus, if the air mass above the inversion was approximately horizontally homogeneous, as might be expected in Willoughby's conceptual model, the increase of eye θ_e observed in Fig. 5 cannot be explained in terms of undilute parcel ascent, but can be explained in terms of horizontal mixing from the eyewall where large values of θ_e were found before the transition.

It is interesting to note that Hurricane Olivia's eyewall was changing from circular to elliptical at the time that we observed the transition in flight-level profiles. Reasor et al. (2000) found that the vorticity profiles across the eye and eyewall of Olivia supported exponential instability during the 25 September flights, and that azimuthal wavenumber two dominated the instability. They proposed this instability and subsequent horizontal vorticity mixing as the causal mechanism for the appearance of Olivia's elliptical eyewall.

Emanuel (1997) argues that a flux of angular momentum from the eyewall to the eye is necessary to explain observed hurricane intensities. Our results offer evidence that angular momentum is often transported from the eyewall to the eye *subsequent* to maximum intensity. Can we find evidence that such transport takes place during intensification? Although the transitions in the kinematic fields between regime 1 and regime 2 have a clear signature in the data when the changes are associated with intensifying versus weakening hurricanes, we did not find a robust signal in the *kinematic* data that would suggest that mixing takes place episodically (or continuously) during intensification. We did find, however, that thermodynamic profiles sometimes transition between regime 1 and 2 during intensification. As an example, consider the thermodynamic structure in Hurricane Olivia during intensification on 24 September (Fig. 13). Profiles of θ_e during the 2040–2103 UTC radial leg inbound–outbound pair were indicative of regime 1 (Fig. 13a). A local θ_e minimum (358 K) was observed near the eye center, and maxima were observed in the eyewall (366 K during the inbound leg and 362 K during the outbound leg). Dewpoints near the eye center were ~4°C. The following radial leg pair (2112–2135 UTC) exhibits nearly monotonic θ_e profiles and is indicative of regime 2 (Fig. 13b). Near the eye center, θ_e had increased to 371 K, and dewpoints had increased to 8°C. Such changes in θ_e near the eye center may be due to horizontal mixing. Another consideration is that the eye air is far from homogeneous and the aircraft measures dramatically different local values from one radial leg pair to another. Given the limitations of the radial leg dataset, we could not reconcile this causal ambiguity.

The appearance of monotonic θ_e profiles in Olivia during intensification is not unique. Considering 463 radial legs flown at 850, 700, 600, and 500 mb, in 21 intensifying hurricanes, we found that ~26% of the profiles exhibited higher θ_e near the eye center than in the eyewall. It should be noted that during the aircraft's

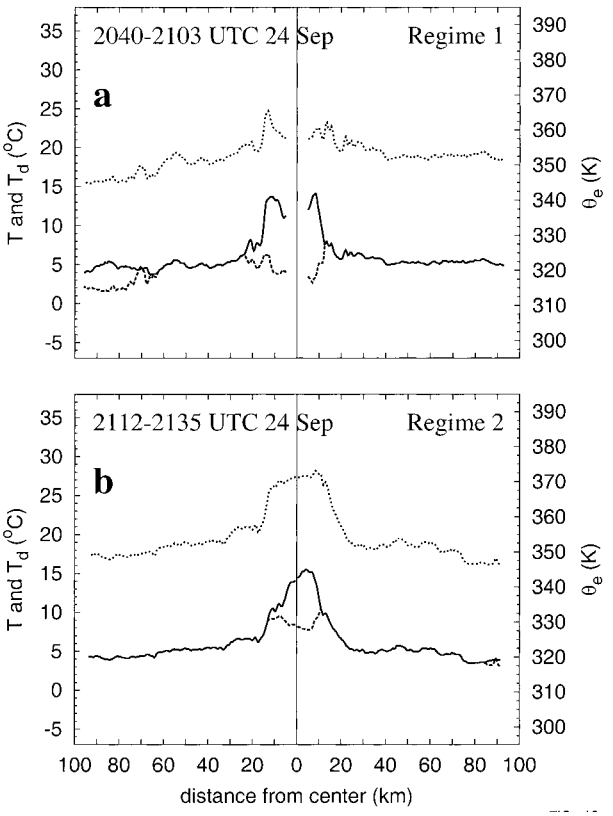

FIG. 13. Thermodynamic profiles observed at 600 mb in Hurricane Olivia (1994) during intensification on 24 Sep. (a) Profiles indicative of regime 1 as the aircraft penetrated the eye at 2052 UTC. (b) Profiles indicative of regime 2 as the aircraft penetrated the eye at 2123 UTC. Near the eye center, θ_e increased from 358 to 371 K in 31 min.

passage through the eyewall, the thermodynamic instrumentation may become wetted, which acts to erroneously reduce temperatures and increase dewpoints. Under such conditions, eyewall θ_e may be underestimated by up to 5 K (Eastin 1999). However, when θ_e errors due to instrument wetting were removed in a subset of radial legs within the flight-level dataset (see Eastin 1999), we still found ~20% of the profiles within intensifying hurricanes exhibited higher θ_e in the eye than the eyewall. Considering the very short time periods over which the transitions between regime 1 and regime 2 can occur, the relevance of nearly instantaneous θ_e cross sections, as found, for example, in Hawkins and Imbembo (1976), may be questionable.

3. Conclusions

We have demonstrated, using flight-level data, that the kinematic and thermodynamic fields across the eye and eyewall of hurricanes are observed to transition between two distinct regimes. In regime 1, angular velocity and vorticity profiles are peaked in the eyewall and relatively depressed in the eye. Dewpoint depressions in the eye are generally large and equivalent potential temperatures (θ_e) are often higher in the eyewall than the eye. The transition to regime 2 is marked by a relaxation of the flow across the eye and eyewall toward solid body rotation, and an increase in dewpoints in the eye. The former causes an increase in the local tangential flow and angular momentum in the eye. The increase in dewpoints causes an increase in θ_e near the eye center, which results in a monotonic θ_e profile with a maximum near the eye center. Generally, regime 1 is indicative of intensifying periods and the transition to regime 2 typically occurs after maximum intensity. The transition can occur in less than 1 h. Evidence that transitions between regime 1 and regime 2 take place during intensification was found in observed changes in θ_e profiles across the eye and eyewall.

Consideration of dropsonde data in Hurricane Olivia (1994) suggested that the transition of equivalent potential temperature from regime 1 to regime 2 cannot be explained solely in terms of ascent within the eye. We did find however that horizontal mixing processes across the eyewall and eye could explain the observed transitions, and the dynamics of the mixing may be understood in a highly idealized 2D barotropic framework. Comparisons were made between vorticity profiles measured by aircraft and results of a numerical integration, and a number of similarities were evident.

Acknowledgments. The authors would like to thank Wayne Schubert, Paul Reasor, Michael Montgomery, Frank Marks, Hugh Willoughby, William Gray, Peter Black, Ricardo Prieto, Mark DeMaria, and David Nolan for their assistance and helpful comments. Ricardo Prieto generously provided the passive tracer code used in section 2c. We are grateful to the flight crews and scientists from NOAA's Aircraft Operations Center, the Hurricane Research Division, and the Air Force 53rd Weather Reconaissance Squadron for their dedicated efforts of the past two decades to collect the flight-level data used in this study. We would also like to thank Hugh Willoughby, Ed Rahn, and Chris Landsea of the Hurricane Research Division for their efforts in making the data available to us. This work was supported by NSF Grant ATM-9729970, NOAA Grant NA67RJ0152 (Amendment 19), and NSF Grant ATM-9616818.

REFERENCES

Black, P. G., and F. D. Marks, 1991: The structure of an eyewall meso-vortex in Hurricane Hugo (1989). *Proc. 19th Conf. on Hurricanes and Tropical Meteorology,* Miami, FL, Amer. Meteor. Soc., 579–582.

Bolton, D., 1980: The computation of equivalent potential temperature. *Mon. Wea. Rev.,* **108,** 1046–1053.

Eastin, M. D., 1999: Instrument wetting errors in hurricanes and a re-examination of inner-core thermodynamics. Atmospheric Science Paper 683, Department of Atmospheric Science, Colorado State University, 203 pp. [Available from Department of Atmospheric Science, Colorado State University, Fort Collins, CO 80523.]

Emanuel, K. A., 1997: Some aspects of hurricane inner-core dynamics and energetics. *J. Atmos. Sci.*, **54,** 1014–1026.

Fletcher, R. D., J. R. Smith, and R. C. Bundgaard, 1961: Superior photographic reconnaissance of tropical cyclones. *Weatherwise*, **14,** 102–109.

Franklin, J. L., S. J. Lord, and F. D. Marks Jr., 1988: Dropwindsonde and radar observations of the eye of Hurricane Gloria (1985). *Mon. Wea. Rev.*, **116,** 1237–1244.

Hawkins, H. F., and S. M. Imbembo, 1976: The structure of a small, intense hurricane—Inez 1966. *Mon. Wea. Rev.*, **104,** 418–442.

Jordan, C. L., 1961: Marked changes in the characteristics of the eye of intense typhoons between the deepening and filling stages. *J. Meteor.*, **18,** 779–789.

Jorgensen, D. P., 1984: Mesoscale and convective-scale characteristics of mature hurricanes. Part I: General observations by research aircraft. *J. Atmos. Sci.*, **41,** 1268–1285.

Kuo, H.-L., 1959: Dynamics of convective vortices and eye formation. *The Atmosphere and Sea in Motion*, B. Bolin, Ed., Rockefeller Institute Press, 413–424.

Malkus, J. S., 1958: On the structure and maintenance of the mature hurricane eye. *J. Meteor.*, **15,** 337–349.

OFCM, 1993: National Hurricane Operations Plan, 125 pp. [Available from Office of the Federal Coordinator for Meteorological Services and Supporting Research, Suite 1500, 8455 Colesville Rd., Silver Spring, MD 20910.]

Reasor, P. D., M. T. Montgomery, F. D. Marks Jr., and J. F. Gamache, 2000: Low-wavenumber structure and evolution of the hurricane inner core observed by airborne dual-Doppler radar. *Mon. Wea. Rev.*, **128,** 1653–1680.

Schubert, W. H., M. T. Montgomery, R. K. Taft, T. A. Guinn, S. R. Fulton, J. P. Kossin, and J. P. Edwards, 1999: Polygonal eyewalls, asymmetric eye contraction, and potential vorticity mixing in hurricanes. *J. Atmos. Sci.*, **56,** 1197–1223.

Willoughby, H. E., 1998: Tropical cyclone eye thermodynamics. *Mon. Wea. Rev.*, **126,** 3053–3067.

——, and P. G. Black, 1996: Hurricane Andrew in Florida: Dynamics of a disaster. *Bull. Amer. Meteor. Soc.*, **77,** 543–549.